ISSN 1392–1207. MECHANIKA. 2023 Volume 29(1): 42–50

Actuation Performance of Macro Fibre Composite (MFC) as Actuator in Vibration Reduction of Cantilever Beams

Ali RAZA*, Swarup MAHATO, Rūta RIMAŠAUSKIENĖ*****
**Kaunas University of Technology, Studentų g. 56, Kaunas, Lithuania, E-mail: ali.raza@ktu.edu*
***Kaunas University of Technology, Studentų g. 56, Kaunas, Lithuania, E-mail: swarup.mahato@ktu.lt*
****Kaunas University of Technology, Studentų g. 56, Kaunas, Lithuania,*
E-mail: ruta.rimasauskiene@ktu.lt (Corresponding author)
crossref http://dx.doi.org/10.5755/j02.mech.31732

1. Introduction

Smart materials have received considerable attention in the field of automation due to their ability to facilitate in measurement and control operations [1]. Piezoelectric materials are frequently employed in energy harvesting, health monitoring and vibration damping etc., due to their strong electromechanical coupling, significant blocking force, high stiffness, and quick response [2–5]. Lead zirconium titanate (PZT), one type of piezoceramic material, has a high structural stiffness that generates large actuation force. The lead-based piezoceramic is widely used in a variety of industrial applications, but it has some limitations, including the brittle nature of ceramic material, low flexibility, and low conformance to curved structures, which can lead to early failure and low stability. Addition to these, the presence of lead, which is banned by the Restriction of Hazardous Substances (RoHS) directive of the European Union, is its main drawback. Due to a new regulation, harmful materials like lead, mercury, cadmium, and hexavalent chromium are banned from use in electronic components[6]. Polyvinylidene fluoride (PVDF) is another widely used piezoelectric material, that is significantly more elastic than piezo ceramics but provides low actuation forces.

The mechanical limitations, mentioned above are mostly alleviated by introducing piezoceramic fibers into ductile polymer matrix [7–9]. Smart Material Corp. is pioneered to develop this type of composite [10]. The second type of Active-Fiber Composite (AFC) actuator, was created by MIT and that was the first composite actuator employed primarily on actuation of structures [9, 11]. The NASA Langley Research Center developed the third type known as Macro Fiber Composite (MFC) in 1999 [12]. The developed MFC is flexible which allows it to easily conform to a curved surface. The other MFCs are mainly composed of piezo-ceramics fibers, matrix material, and electrodes with d31 and d33 configuration modes. In MFC-d31 polarization of piezoelectric material occurs perpendicular to the piezo-ceramics fibers orientation, while in MFC-d33 the polarization occurs parallel to the orientation of the piezo fiber. As a result, MFC-d33 can generate actuation forces using the d33 effect, which is often significantly larger (approximately 2 times) than the d31 effect. Due to these unique features of piezoelectric fiber composites, significant work has already been done to incorporating this smart material with structures for health monitoring and vibration control [3, 9, 10, 13]. Pandey and Arockiarajan did an intensive study on MFCs to investigate their actuation performance. A 2-dimensional model based on Kirchhoff plate theory was created using ABAQUS platform, and numerical simulation was done on the model to validate it with experimental results for MFC bonded with uni-morph structure. The bimorph configuration was investigated using this methodology. Parametric studies were also conducted and presented to study the effect of thickness of plate and piezo-electric fibers orientation on MFCs performance. [14]. Shun-Qi Zhang et al. developed a finite element model of thin-walled smart composite integrated with MFCs (d33and d31 types) having different piezo fiber orientations. The actuation effect of MFC-d33 and MFC-d31 on smart composite were examined. The finite element model was confirmed with results obtained from a cantilever plate structure integrated with MFCs (d33 and d31) patch-es. Furthermore, the simulation results also confirm that the d33 patch generates actuation force approximately two times higher than d31 patch [9]. Yu Shi et al. proposed a new bonding technique to integrate the PZT energy harvesting element (MFC-8528, P2) onto the surface of the carbon fiber composite (CFC) airframe. A vacuum bag system and a co-curing technique were used to fabricate the MFC on the CFC surface. To verify the efficiency of the proposed bonding technique, vibration tests were per-formed to compare the energy harvested by the proposed technique with direct mechanical bonding method. The findings showed that the proposed methodology is more effective than direct bonding. [15]. W.K. Miao et al. per-formed an investigation to control the active vibrations of the cantilever beam by using MFC actuators and sensors. Two MFCs patch were applied for active control of the cantilever beam, and the third patch was applied as a sensor. The active vibration control (AVC) of the first two vibration modes was executed by applying the proportional derivative (PD) control algorithm and the fuzzy control algorithm. The results showed that the vibrations of the first two modes of beams were effectively suppressed by MFC actuators and sensor. The techniques used in the experiments can be implemented in different fields to control vibrations [16]. Cihang Xie et al. reported on the active vibration control of the lattice grid beam using piezoelectric fiber composite as actuator. A new AVC methodology was applied using the fractional order PDμ algorithm to suppress the vibration in beam and simulation was performed on the beam, when it is subjected to a variety of dynamic loads including harmonic excitation, step excitation and initial disturbance etc. So, it has been proven that vibration amplitude can be suppressed more dramatically and quickly while using the suggested control methodology compared to the traditional integer-order PD technique[17] . Marinangeli et al.

did work on the active vibration control (AVC) of a CFC plate having free edges. A modal vibration exciter was used to excite the plate out of the plane, and MFC transducers were integrated with plate to damp the vibrations. The MFCs based actuators and sensors were placed on the plate using the maximal modal strain rule to suppress the vibrations in second natural mode. The second mode of vibration could be effectively controlled using both integer and fractional-order positive position feedback (PPF). The proposed fractional-order controller technique was found to be more efficient in terms of obtaining the same efficiency with a lower actuation voltage. Furthermore, the results validate a positive performance in reducing the spill over effect caused by uncontrolled modes [18]. Jaroslaw Gawryluk et al. carried out extensive research on the vibration amplitude reduction of the cantilever composite beam. Numerical studies and experiments were performed on the composite beam integrated with the MFC-8528-P1 actuator. The proportional (P), derivative (D) and PD controls algorithms were implemented to control the vibration and to determine the time constant and validate the proposed idea. Moreover, the finite model of composite beam was developed by using ABAQUS software, and control algorithms were implemented on the model to check the possibilities of vibration reduction. The experimental and numerical results verified that the control algorithms have a significant effect on vibration amplitude reduction of beam [19].

After reviewing the extensive literature, the authors conclude that there is a lack of a quantified comparative study on the use of MFC actuator over various engineering materials in the vibration reduction field. This motivates the current work to use MFC controllers with three types of materials in vibration control applications. These materials are Polylactic acid (PLA), PLA with short carbon fibers (PLA-SCF), and PLA with continuous carbon fibers (PLA-CCF). In this work, MFC8507-P2 [10] is integrated with cantilever beam and the finite element (FE) model of beam is created with three different aforementioned material properties in ANSYS software. To limit the dynamic amplitude of the vibrating cantilever beam, variable voltages are provided to integrated MFC8507-P2 patch and the actuation performance is studied.

2. Control model and MFC details

The basic model for actuator-based control and MFC actuator details are discussed here.

2.1. Vibration control strategy for linear system

A linear system with controller is represented by a set of differential equations. The state-space representation is widely used model to describe the control system and it is given as follow [20]:

$$\dot{\boldsymbol{x}}(t) = \boldsymbol{A}\boldsymbol{x}(t) + \boldsymbol{B}\boldsymbol{f}(t), \tag{1}$$

$$\boldsymbol{y}(t) = \boldsymbol{C}\boldsymbol{x}(t) + \boldsymbol{D}\boldsymbol{f}(t). \tag{2}$$

The state vector represented by $\boldsymbol{x}(t)$ and $\dot{\boldsymbol{x}}(t)$ is the differentiation of it respect to time t. The state vector consists of displacement and velocity in the above equations. The time-varying input and output vectors are represented as $\boldsymbol{f}(t)$ and $\boldsymbol{y}(t)$, respectively. $\boldsymbol{f}(t)$ can be either the external excitation only or excitation with feedback control force. $\boldsymbol{A}$ and $\boldsymbol{B}$ are known as system and input matrix, respectively. These two matrixes are constant for a time-invariant linear structure. The system matric $\boldsymbol{A}$ convey the information about mass, stiffness and damping of the system in case of a dynamic structure whereas input matric $\boldsymbol{B}$ carries the information of location of external forces. The $\boldsymbol{C}$ and $\boldsymbol{D}$ are observed matrix and feed through matrix, respectively. Similar to the $\boldsymbol{B}$, feedthrough matrix $\boldsymbol{D}$ determines the location of controlling forces. If a zero initial condition, i.e. $\boldsymbol{x}(t = =0)=0$ applies in Eqs. (1) and (2), one may derive the output-input relation using the Laplace transform as follows:

$$\boldsymbol{y}(s) = \left[\boldsymbol{C}(s\boldsymbol{I} - \boldsymbol{A})^{-1}\boldsymbol{B} + \boldsymbol{D}\right]\boldsymbol{f}(s) = \boldsymbol{H}(s)\,\boldsymbol{f}(s). \tag{3}$$

$\boldsymbol{H}(s)$ donates the transfer function of the system in a single input and single output (SISO) system, while it is considered transfer matrix in case of multi-input and multi output (MIMO) system as it given here:

$$\boldsymbol{H}(s) = \left[\boldsymbol{C}(s\boldsymbol{I} - \boldsymbol{A})^{-1}\boldsymbol{B} + \boldsymbol{D}\right]. \tag{4}$$

where: s is the complex variable in Laplace domain and $\boldsymbol{I}$ is the identity matrix. By following above mentioned formulation, infinite modes should be controlled simultaneously for a beam structure, but it may not be possible to control all the modes simultaneously in practice. In order to control vibrations, the actuators are often integrated with the system to lower the amplitudes of few initial modes. The leftover modes are categorized as residual modes. This approach works for most of the scenario.

Now, the dynamic equilibrium equation for a discretized system can be expressed as:

$$\boldsymbol{M}\ddot{\boldsymbol{x}}(t) + \boldsymbol{C}\dot{\boldsymbol{x}}(t) + \boldsymbol{K}\boldsymbol{x}(t) = \boldsymbol{f}(t). \tag{5}$$

The mass $\boldsymbol{M}$, damping $\boldsymbol{C}$, and stiffness $\boldsymbol{K}$ matrices can be derived using analytical, numerical, or experimental approaches. The input vector $\boldsymbol{f}(t)$ works here as exciter. The coupled equilibrium equation of motion can be decoupled using an orthogonal transformation into its modal coordinates:

$$\boldsymbol{x}(t) = \sum_{j=1}^{\infty} \boldsymbol{\Phi}_j \boldsymbol{\eta}_j(t), \tag{6}$$

where: $\boldsymbol{\Phi}_j$ represents mode shape and modal response given by $\boldsymbol{\eta}_j(t)$. By taking advantage of linear structure, total response is presented as superposition of modal responses. Using above orthogonal transformation in Eq. (5), the equilibrium equation in modal coordinates would be as follow:

$$\ddot{\boldsymbol{\eta}}_j(t) + 2\zeta\omega_n\dot{\boldsymbol{\eta}}_j(t) + \omega_n^2\boldsymbol{\eta}_j(t) = \boldsymbol{\mu}^{-1}\boldsymbol{\Phi}_j\boldsymbol{f}(t). \tag{7}$$

The modal mass matrix is represented by $\boldsymbol{\mu}$. In the above equation, the modal damping and natural frequency ratio are given by ζ and ω_n, respectively. Using the above equation, one can rewrite the Eq. (1) as given bellow:

$$\begin{bmatrix}\dot{\boldsymbol{\eta}}\\ \ddot{\boldsymbol{\eta}}\end{bmatrix}=\begin{bmatrix}\boldsymbol{0}_{n\times n} & \boldsymbol{I}_{n\times n}\\ -\omega_n^2 & -2\zeta\omega_n\end{bmatrix}\begin{bmatrix}\boldsymbol{\eta}\\ \dot{\boldsymbol{\eta}}\end{bmatrix}+\begin{bmatrix}\boldsymbol{0}_{n\times 1}\\ \boldsymbol{\mu}^{-1}\boldsymbol{\Phi}_j\end{bmatrix}\boldsymbol{f}. \quad (8)$$

Again Eq. (2) can be obtained for three different outputs as given here:

a) Displacement:

$$\boldsymbol{y}=\begin{bmatrix}\boldsymbol{\Phi}_j & \boldsymbol{0}_{n\times n}\end{bmatrix}\begin{bmatrix}\boldsymbol{\eta}\\ \dot{\boldsymbol{\eta}}\end{bmatrix}. \quad (9)$$

b) Velocity:

$$\boldsymbol{y}=\begin{bmatrix}\boldsymbol{0}_{n\times 1} & \boldsymbol{\Phi}_j\end{bmatrix}\begin{bmatrix}\boldsymbol{\eta}\\ \dot{\boldsymbol{\eta}}\end{bmatrix}. \quad (10)$$

c) Acceleration:

$$\boldsymbol{y}=\begin{bmatrix}-\boldsymbol{\Phi}_j\omega_n^2 & -2\boldsymbol{\Phi}_j\zeta\omega\end{bmatrix}\begin{bmatrix}\boldsymbol{\eta}\\ \dot{\boldsymbol{\eta}}\end{bmatrix}+\boldsymbol{\Phi}_j\mu^{-1}\boldsymbol{\Phi}_j^T\boldsymbol{f}. \quad (11)$$

2.2. Constitutive equations for MFC

The MFC actuator, used here i.e. MFC8507-P2 is made up of seven different layers, including one active layer and two acrylic and kapton electrode layers positioned on top and bottom of the active layer, respectively [7]. Piezoelectric fibres are incorporated into a structural epoxy matrix in the active layer. The electrode layer is made up of interdigitated copper rods embedded in an epoxy matrix. The MFC may conform to the curved surface due to the flexibility of the epoxy that surrounds the fibers and copper rods. The protective layers for the MFC are made of acrylic and kapton films. MFCs can be categorized as d33 (P1 type) and d31(P2 type), depending on the orientation of fibers and poling directions. The poling direction and applied electric field are both parallel to the fibre orientation in the d33 type. While in the d31 type, the poling direction and the applied electric field are perpendicular to the fiber orientation. The 0° fibre orientation is commonly found in both types of (d33 and d31) of MFC. The constitutive equations of piezoelectric materials, with σ and D as dependent variables and $\varepsilon$and E as independent variables, can define the sensing and actuation performance of MFCs as expressed below:

$$\boldsymbol{\sigma}_{ij}=\boldsymbol{c}_{ijkl}^{E}\boldsymbol{\varepsilon}_{kl}-\boldsymbol{e}_{kij}\boldsymbol{E}_k, \quad (12)$$

$$\boldsymbol{D}_n=\boldsymbol{e}_{nj}^{T}\boldsymbol{\varepsilon}_j-\boldsymbol{X}_{kn}^{\varepsilon}\boldsymbol{E}_k. \quad (13)$$

The description of the Eqs. (12) and (13) and derivation of matrices from these equations cab be found in literature [7]. In d33, the electric field is applied in thickness direction due to the electrode configuration. So, the constitutive equation for d31 type MFC would be as below [7]:

$$\boldsymbol{D}_3=\begin{bmatrix}e_{xx} & e_{xy} & 0 & 0 & 0\end{bmatrix}\begin{bmatrix}\varepsilon_{xx} & \varepsilon_{yy} & \gamma_{xy} & \gamma_{yz} & \gamma_{xz}\end{bmatrix}+X_{xx}E_x. \quad (14)$$

3. Finite element modelling of the system

The current design study, includes a piezoelectric microfiber composite (MFC8507-P2) as an actuator integrated on a cantilever beam. The cantilever beam is modeled with three various mechanical properties, i.e. PLA, PLA-SCF, and PLA-CCF individually. The whole system is modeled in the ANSYS software and the control performance is observed by tuning the voltages, supplied to the MFC actuator.

3.1. Details of beam with MFC actuator

The Finite Element Model (FEM) analysis has been used to simulate the dynamic characteristic of the composite structure. In current proposed study, ANSYS / Workbench platform has been used to model the cantilever beam of size 120 mm×20 mm×1.35 mm with a MFC-8507P2 as actuator of active size 85 mm×7 mm×0.3 mm [10, 21]. The geometrical features of cantilever beam and MFC-8507P2 to define 3D geometry are presented in Fig. 1.

The mechanical properties of the materials have been presented in Table 1 and the material properties of the MFC patch are given in Table 2. The 20-node quadratic brick SOLID 186 and SOLID226 have been implemented for the cantilever beam and MFC actuator respectively. The SOLID226 elements solve the constitutive equations for an elastic piezoelectric solid. In addition, to improve the solution accuracy of the 20-node quadratic elements in modelling of highly curved structures, it is recommended to utilize 20-node elements throughout when element types are integrated within a single model to ensure that each node on adjacent elements coincides. The element density for the modal is sufficient to properly evaluate the behaviour of the beam and it is investigated that further mesh refinement has no considerable effect on the beam's dynamics behaviour [22]. After modelling the geometry, proper meshing has been carried out until little or no further changes in the computed natural frequency are observed. The goal of a refine meshing is to get more accurate findings, but using an excessively fine mesh will take longer time to calculate the required output, making it unsuitable to use. The current model includes a total of 400 SOLID186 elements for the beam and 102 elements within the MFC volume. The MFC8507-P2 patch has been integrated with cantilever beam, at 10 mm away from the fixed end of the cantilever beam, and the connection between the MFC8507-P2 patch and the cantilever beam is of the bonded type.

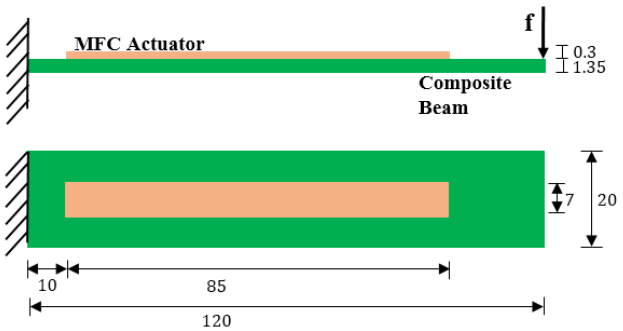

Fig. 1 View of cantilever beam with bonded MFC-8507P2

Table 1

Mechanical Properties of PLA, PLA-SCF and PLA-CCF [23–25]

Characteristics	PLA	PLA-SCF	PLA-CCF
Density, kg/m^3	1240	1350	1552
Young's modulus, MPa	3500	7541	25940
Poisson's ratio	0.36	0.4	0.24
Shear modulus, MPa	1286	2693	4950
Tensile strength, MPa	54.7	53.4	245.4

Table 2

Material properties of MFC8507-P2 [9, 10, 14, 15, 26]

Characteristics	MFC-8507P2
Young's modulus, GPa	Ẽ3=30.336
	Ẽ3=Ẽ1=15.857
Shear modulus, GPa	Ĝ12=Ĝ13=5.515
	Ĝ23= 5.515
Poisson's ratio	ṽ12=ṽ13=0.31
	ṽ23=0.438
Piezoelectric dielectric constant, pC/N	d̃31= -170
	d̃32= -100
Density, kg/m^3	5400

4. Results and discussions

The system is characterized by its modal behaviour, and then the amplitude reduction efficiency has been tested under varying currents to the actuator. The final results are presented in the article.

4.1. Calculation of mode shape and natural frequencies

The first part of the numerical simulation analysis was dedicated to determine the natural frequencies and mode shapes of the cantilever beam. The first eight natural frequencies of the beams made of PLA, PLA-SCF, and PLA-CCF are presented in Table 3. The mass and stiffness of each material increase slightly due to the addition of MFC8507-P2 patch, and thus the natural frequencies of the beams are differing from actual cantilever beam. From Fig. 2, it can be observed that modes 1, 2, 5, 7 and 8 are bending modes (symmetric modes) and modes 3, 4, and 6 are torsional modes (asymmetric modes) for beams made of PLA and PLA-SCF. While for PLA-CCF, modes 1, 3, 6 and 8 are bending modes (symmetric modes) and mode 4 is translational and 2, 5 and 7 are torsional modes. As observed from the Table 3, the initial modes are bending thus the proposed controlled algorithm is focused to restrain the amplitude of bending modes. Therefore, only bending modes of the cantilever beams made of PLA, PLA-SCF, and PLA-CCF are presented in Fig. 2. The Table 3 summarizes the modal frequencies cantilever beams made of PLA, PLA-SCF, and PLA-CCF, and it can be observed that the modal frequencies increase from PLA to PLA-SCF to PLA-CCF. The natural frequencies of the material depend on their mechanical characteristics i.e., mass and stiffness of the structure. The structure with higher stiffness and lighter mass is considered to have higher resonance modal frequencies value [27, 28]. It can be confirmed from Table 2 that PLA-CCF has the maximum stiffness, while PLA has the minimum and PLA-SCF has intermediate stiffness.

4.2. Estimation of amplitude reduction

The further step of this numerical simulation analysis has been dedicated to check the effect of MFC8507-P2 patch on the vibrating cantilever beam to limit the response amplitudes.

First, transient analysis is performed to estimate overall reduction. One may obtain the interested responses by following Eqs. (1), (2), (9), (10) and (11). Here, the displacement responses are estimated by Eq. (9). The variable voltages, i.e., 0 mV, 2 mV, 4 mV and 6 mV, are supplied to the actuator (MFC8507-P2) and at the same time 0.1 mN impact load is applied at the free end of each cantilever beam individually. The variations in responses are recorded and the amplitude reduction factor is calculated in two approach - on peak-to-peak (PP) and root mean square (RMS). The PP approach gives the local information regarding the reduction while RMS approach gives the overall reduction factor. The transient responses of beams made of PLA, PLA-SCF and PLA-CCF have been presented in Figs. 3, 4, and 5, respectively. Table 4 presents the maximum and RMS amplitude of the displacement responses. From Figs. 3, 4, and 5, it is clear that with increment of actuation voltage, the controlling force is increasing as explained in Eq. (2). Thus, the amplitude of the vibration is reducing. The amplitude reduction for PP values for cantilever beams made of PLA, PLA-SCF and PLA-CCF varies, from 9.52% to 28.57%, 14.29% to 29.68%, and 10.4 3% to 31.32%, respectively, when the supplied voltage varies from 2 mV to 6 mV. While, the amplitude reduction in case of RMS values for cantilever beams made from PLA, PLA-SCF and PLA-CCF varies, from 7.24% to 18.55%, 9.12% to 22.94% and 10.45% to 31.42% respectively as supplied voltage varies, 2 mV to 6 mV.

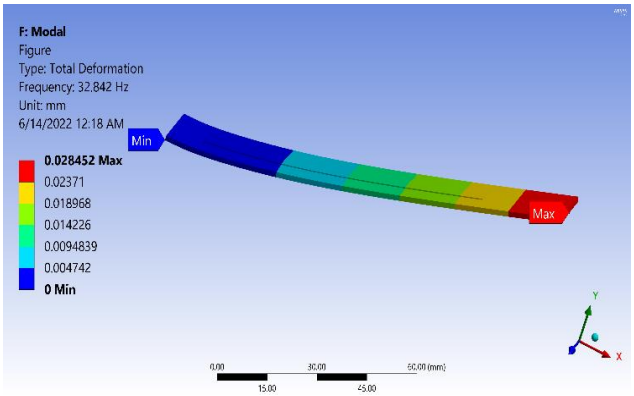

1st bending mode beam made of PLA

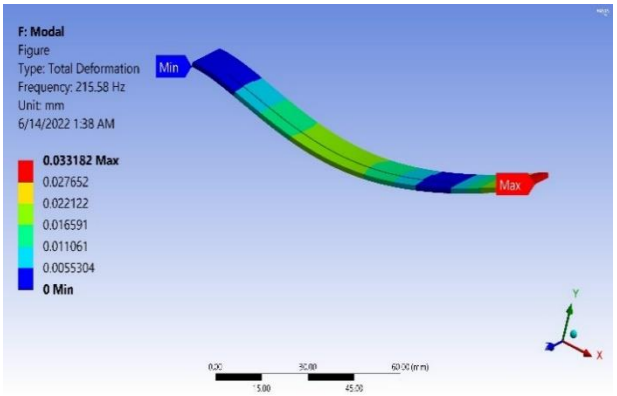

2nd bending mode of beam made of PLA

Fig. 2 Bending mode shapes of cantilever beams made of PLA, PLA-SCF and PLA-CCF

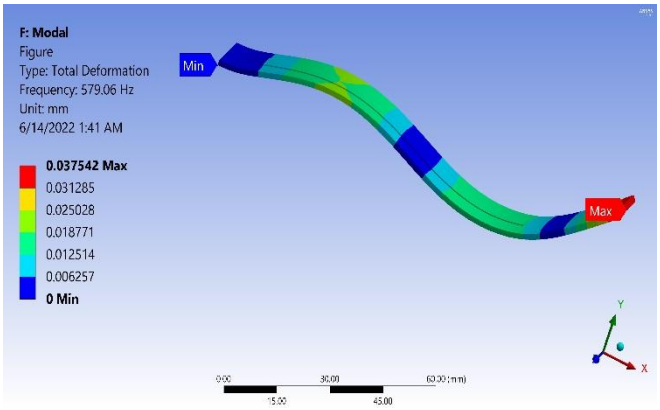

3rd bending mode of beam made of PLA

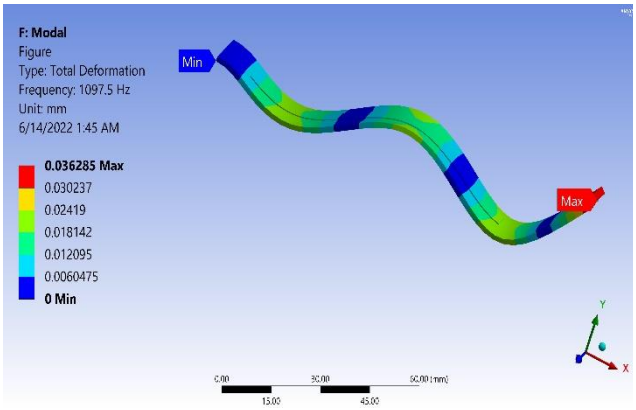

4th bending mode of beam made of PLA

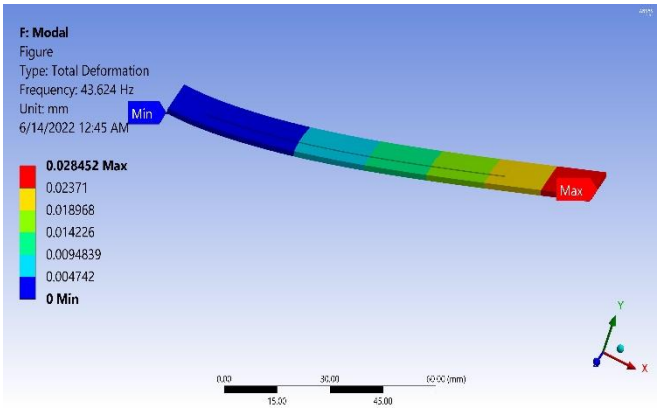

1st bending mode of beam made of PLA-SCF

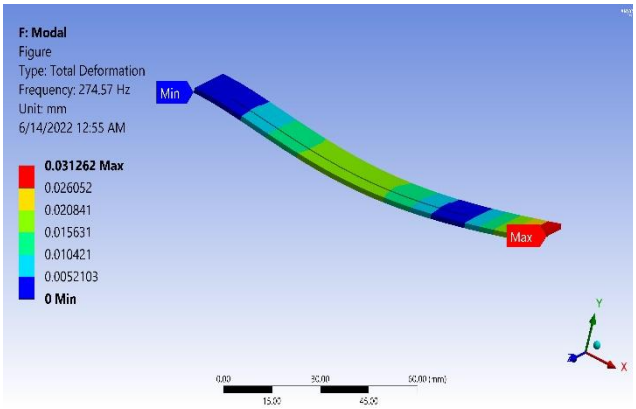

2nd bending mode of beam made of PLA-SCF

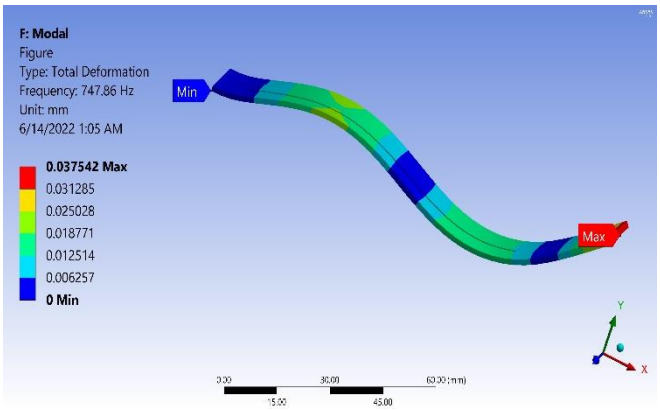

3rd bending mode of cantilever beam made of PLA-SCF

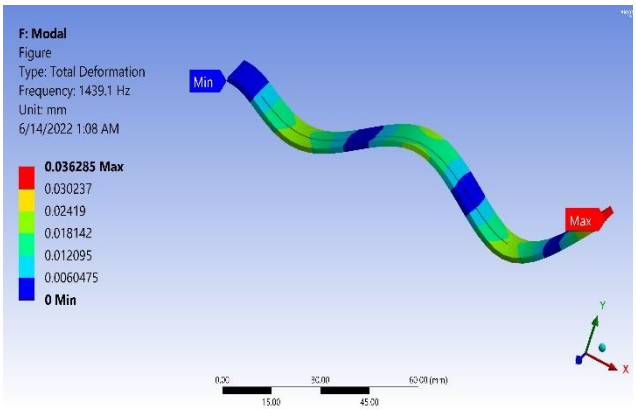

4th bending mode of cantilever beam made of PLA-SCF

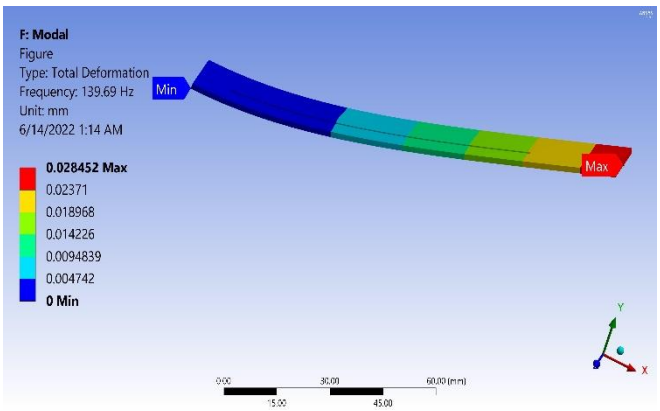

1st bending mode of beam made of PLA-CCF

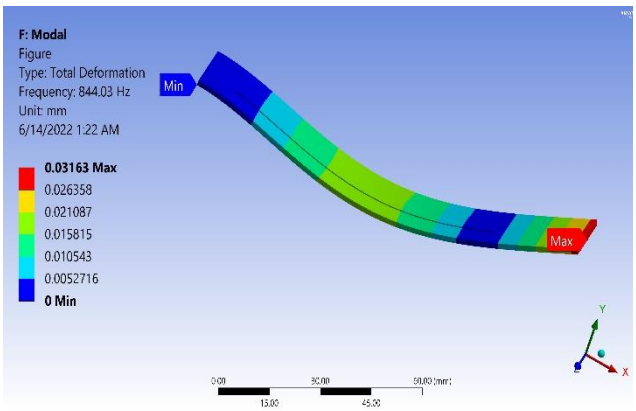

2nd bending mode of beam made of PLA-CCF

Fig. 2 Continuation

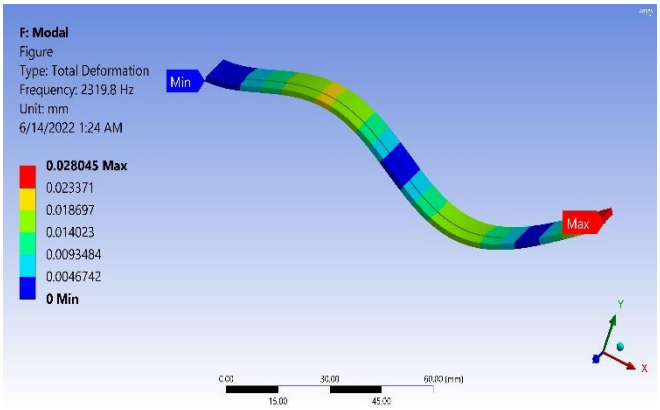

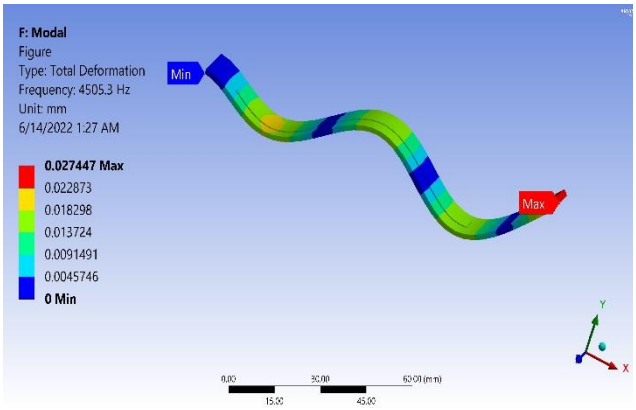

3rd bending mode of beam made of PLA-CCF

4th bending mode of beam made of PLA-CCF

Fig. 2 Continuation

Table 3

Mode shapes of cantilever beam made of PLA, PLA-SCF and PLA-CCF

Mode	PLA		PLA-SCF		PLA-CCF	
	Frequency, Hz	Mode shape	Frequency, Hz	Mode shape	Frequency, Hz	Mode shape
1	32.842	1st bending	43.624	1st bending	139.69	1st bending
2	215.58	2nd bending	274.57	2nd bending	631.14	1st torsional
3	355.43	1st torsional	483.25	1st torsional	844.03	2nd bending
4	380.43	2nd torsional	502.07	2nd torsional	1739.8	1st translational
5	579.06	3rd bending	747.86	3rd bending	1990.4	2nd torsional
6	1096.9	3rd torsional	1432.8	3rd torsional	2319.8	3rd bending
7	1097.5	4th bending	1439.1	4th bending	3739.0	3rd torsional
8	1796.1	5th bending	2360.3	5th bending	4505.3	4th bending

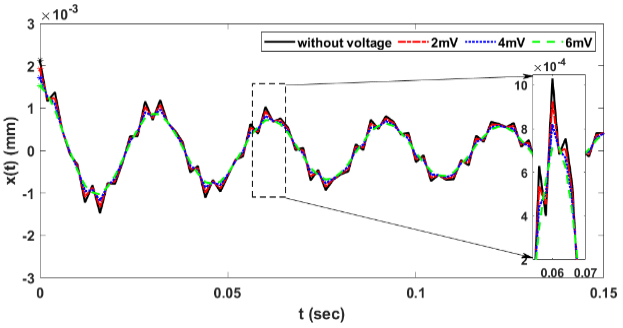

Fig. 3 Vibration response for cantilever beam made of PLA with different control voltage

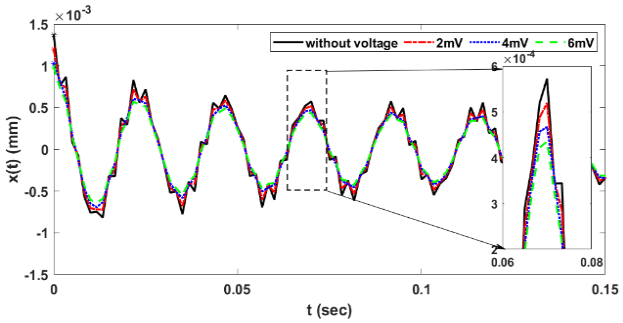

Fig. 4 Vibration response for cantilever beam made of PLA-SCF with different control voltage

The transient analysis gives an overall amplitude reduction information. Thus, to investigate the reduction factor in modal coordinate, the frequency response analysis is performed as the mode by mode inspection reveals more details [29–31] . In practical scenario, it has been observed that the highest displacement of the vibrating beam occurs at the first natural frequency, mostly [21]. Therefore, in this study, the first two modes of two samples (i.e., PLA and PLA-SCF) and only the first mode of PLA-CCF are targeted in order to reduce the vibrating amplitude of the beam. The reason to select only the 1st mode of PLA-CCF is that the 2nd resonance frequency mode appears at high frequency (844 Hz), which is beyond our interest and observation.

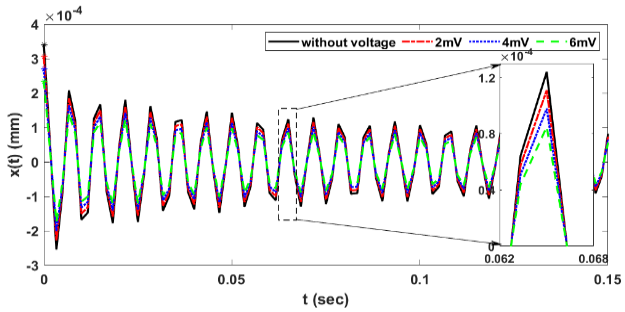

Fig. 5 Vibration response for cantilever beam made of PLA-CCF with different control voltage

Table 4

Vibration amplitude in cantilever beams made of PLA, PLA-SCF and PLA-CCF in time domain

Volt-age, mV	PLA, µm		PLA-SCF, µm		PLA-CCF, µm	
	X_{max}	RMS	X_{max}	RMS	X_{max}	RMS
0	2.130	0.355	1.3719	0.2486	0.3410	0.0520
2	1.924	0.330	1.1991	0.2261	0.3054	0.0466
4	1.723	0.308	1.0316	0.2070	0.2697	0.0411
6	1.532	0.290	0.9846	0.1919	0.2342	0.0357

In frequency domain analysis, variable voltages, i.e., 0 v, 2 mV, 4 mV and 6 mV, are supplied to the

MFC8507-P2 patch and at the same time 0.1 mN load is applied at the free end of each beam individually. After applying variable voltages to the MFC8507-P2 actuator, the amplitude reduction on the corresponding voltages for cantilever beams made of PLA, PLA-SCF and PLA-CCF are obtained. The amplitude reductions for cantilever beams made of PLA, PLA-SCF and PLA-CCF have been presented in the inset portions of Figs. 6 – 8, respectively. Table 5 summarizes the amplitude reduction for cantilever beams made of PLA, PLA-SCF and PLA-CCF with respect to increasing voltages. In case of first mode, we observe improvement in amplitude reductions for the beam made of PLA, PLA-SCF and LA-CCF, 4.28% to 12.84%, 6.49% to 19.495 and 10.34% to 31.32 respectively when supplied voltage varies from 2mV to 6mV in MFC8507-P2 patch. However, in the second resonant modes of beam of PLA and PLA-SCF, a significant decrease in amplitude is observed.

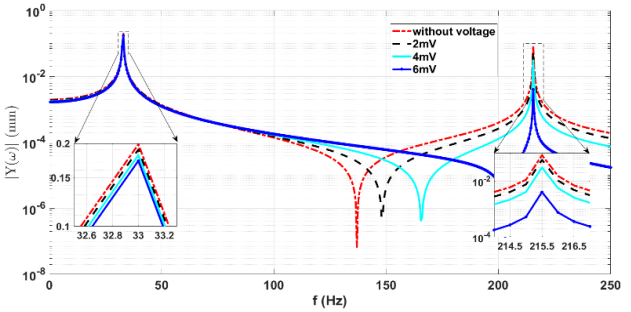

Fig. 6 Amplitude spectrum of cantilever beam made of PLA

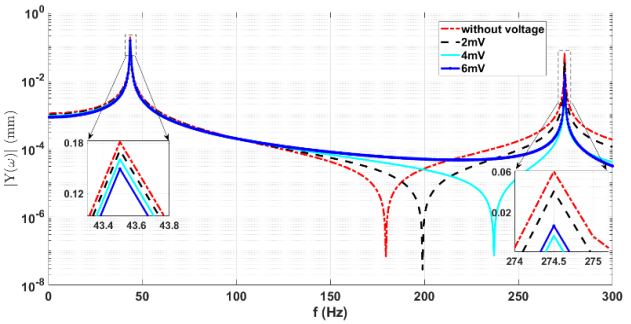

Fig. 7 Amplitude spectrum of cantilever beam made of PLA-SCF

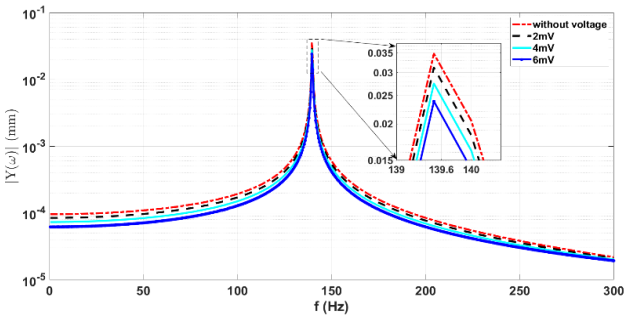

Fig. 8 Amplitude spectrum of cantilever beam made of PLA-CCF

By comparing the amplitude reduction factor for mode by mode, from Fig. 9, it is evident that the vibration of mode 2 is more suppressed with this control strategy. As given in Eq. (2), by changing the feedback matrix, the location of control force can be altered.

By comparing the time domain and frequency domain analysis, it is observed that the RMS values (time domain) are more consistent as it gives the overall information and it supported by the mode by mode reduction inspection. It can be confirmed from the results that the cantilever beam made of PLA-CCF exhibits the highest amplitude reduction, while the cantilever beam made of PLA-SCF and PLA show intermediate and lowest amplitude reduction. The results confirm that a higher stiffer material could increase the actuation performance of MFC8507-P2 patch in application of vibration control.

Table 5

Modal amplitude in cantilever beam made of PLA, PLA-SCF and PLA-CCF in frequency domain

Voltage, mV	PLA, µm		PLA-SCF, µm		PLA-CCF, µm
	Mode1	Mode2	Mode1	Mode2	Mode 1
0.0	199	84	182	61	35
2.0	190	57	170	36	31
4.0	182	30	158	11	28
6.0	173	4	146	14	24

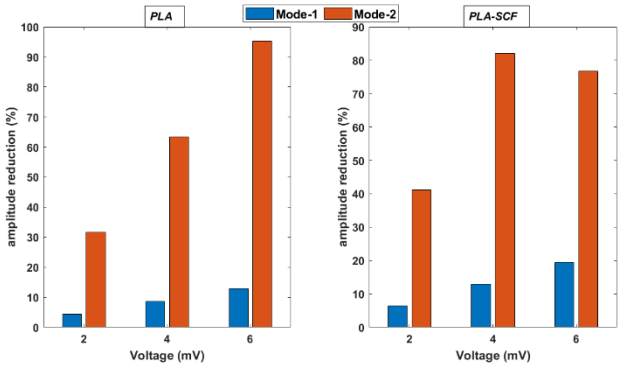

Fig. 9 Comparison of mode by mode amplitude reduction of cantilever beam made of PLA and PLA-SCF

5. Conclusions

Based on the results demonstrated in article, the following conclusion has been drawn:

1. The amplitude reduction in PP values of amplitude reduction for cantilever beam made of PLA, PLA-SCF and PLA-CCF was found from 9.52% to 28.57%, 14.29% to 29.68%, and 10.43% to 31.32%, respectively over time, when the supplied voltage varies from 2 mV to 6 mV in MFC8507-P2 patch Whereas, the vibration reduction in case of RMS for cantilever beam made of PLA, PLA-SCF and PLA-CCF is found, from 7.24% to 18.55%, 9.12% to 22.94% and 10.4 5% to 31.4 2% respectively as supplied voltage varies, 2 mV to 6 mV.

2. In frequency domain amplitude reduction factor is calculated mode by mode for cantilever beam made of PLA, PLA-SCF and PLA-CCF. In case of first mode of cantilever beam made of PLA, PLA-SCF and PLA-CCF, the amplitude reduction varies from 4.28% to 12.84%, 6.49% to 19.495 and 10.34% to 31.32, respectively, when supplied voltages are provided from 2 mV to 6 mV to MFC8507-P2 patch. While in case of second mode of cantilever beam made of PLA and PLA-SCF, the amplitude reduction is very rapid because the amplitudes for second resonant modes are very small and do not have dominant effect on vibrations.

3. The time domain and frequency domain results confirm that the RMS values are more consistent and robust

with the frequency domain values as compared to PP values of vibrating beams.

4. Moreover, the results show that an MFC-based actuator performs better in vibration control for the material that has high stiffness. In the study, it is found that the MFC actuator is best suitable for cantilever beam made of PLA-CCF. As the amplitude of the vibration in cantilever beam made of PLA and PLA-SCF is higher (compare to PLA-CCF), it becomes more difficult to reduce the amplitude by this type of actuator.

The authors are planning to carry out this study with experimental validation and communicate the findings in near future.

References

1. **Leo, D. J.** 2008. Engineering Analysis of Smart Material Systems, John Wiley & Sons, Inc. 576 p.
2. **Takeuchi, K.; Fujino, M.; Suga, T.; Gatty, H. K.; Schröder, S.; Nagendra Kumar, D.; Raja, S.; Ikeda, T.** 2007. Active vibration control of smart plates with partially debonded multilayered PZT actuators, Smart Materials and Structures 16(5): 1584-1594. https://doi.org/10.1088/0964-1726/16/5/012.
3. **Konka, H. P.; Wahab, M. A.; Lian, K.** 2013. Piezoelectric fiber composite transducers for health monitoring in composite structures, Sensors and Actuators, A: Physical 194: 84-94. https://doi.org/10.1016/J.SNA.2012.12.039.
4. **Kim, H. S.; Kim, J. H.; Kim, J.** 2011. A review of piezoelectric energy harvesting based on vibration. International Journal of Precision Engineering and Manufacturing, 12(6): 1129–1141. https://doi.org/10.1007/S12541-011-0151-3.
5. **Smith, R**. 2005. Smart material systems, model development. Society for Industrial and Applied Mathematics, 528 p.
6. **Fasquelle, D.; Mascot, M.; Sama, N.; Remiens, D.; Carru, J. C.** 2015. Lead-free piezoelectric thin films for RoHS devices, Sensors Actuators A: Physical 229:, 30–35. https://doi.org/10.1016/J.SNA.2015.02.009.
7. **Pandey, A.; Arockiarajan, A.** 2016. Actuation performance of macro-fiber composite (MFC): Modeling and experimental studies, Sensors Actuators A: Physical, p. 114–129. https://doi.org/10.1016/J.SNA.2016.07.022.
8. **Topolov, V. Y.; Bisegna, P.; Bowen, C. R**. 2014. Piezo-active composites: Orientation effects and anisotropyfactors, Springer, p.185. https://doi.org/10.1007/978-3-642-38354-0.
9. **Zhang, S. Q.; Li, Y. X.; Schmidt, R**. 2015. Modeling and simulation of macro-fiber composite layered smart structures, Composite Structures 126: 89–100. https://doi.org/10.1016/J.COMPSTRUCT.2015.02.051.
10. Smart Material, [accessed 13 May 2022]. Available from Internet: https://www.smart-material.com/
11. **Williams, R. B.; Grimsley, B. W.; Inman, D. J.; Wilkie, W. K.** 2008. Manufacturing and Mechanics-based characterization of macro fiber composite actuators, ASME International Mechanical Engineering Congress and Exposition, p. 79–89. https://doi.org/10.1115/IMECE2002-39005.
12. NASA, [accessed 13 May 2022, Available from interner:https://www.nasa.gov/
13. **Choi, S. C.; Park, J. S.; Kim, J. H.** 2007. Vibration control of pre-twisted rotating composite thin-walled beams with piezoelectric fiber composites, Journal of Sound and Vibration 300: 176–196. https://doi.org/10.1016/J.JSV.2006.07.051.
14. **Pandey, A.; Arockiarajan, A.** 2016. Actuation performance of macro-fiber composite (MFC), Modeling and experimental studies, Sensors Actuators A: Physical, p. 114–129. https://doi.org/10.1016/J.SNA.2016.07.022.
15. **Shi, Y.; Hallett, S. R.; Zhu, M.** 2017. Energy harvesting behaviour for aircraft composites structures using macro-fibre composite: Part I – Integration and experiment, Composite Strucures 160: 1279–1286. https://doi.org/10.1016/J.COMPSTRUCT.2016.11.037.
16. **Miao, W. K.; Xu, M. L.; Wu, C. S**. 2014. Active vibration control of cantilever beam using MFC sensor and actuator, Recent Advances in Structural Integrity Analysis - Proceedings of the International Congress, p. 447–452. https://doi.org/10.1533/9780081002254.447.
17. **Xie, C.; Wu, Y.; Liu, Z.** 2018. Modeling and active vibration control of lattice grid beam with piezoelectric fiber composite using fractional order PDμ algorithm, Composite-Structures 198: 126–134. https://doi.org/10.1016/j.compstruct.2018.05.060.
18. **Marinangeli, L.; Alijani, F.; HosseinNia, S. H.** 2018. Fractional-order positive position feedback compensator for active vibration control of a smart composite plate. Journal of Sound and Vibration 412: 1–16. https://doi.org/10.1016/j.jsv.2017.09.009.
19. **Gawryluk, J.; Mitura, A.; Teter, A**. 2020. Dynamic control of kinematically excited laminated, thin-walled beam using macro fibre composite actuator, Composite Structures, p. 236. https://doi.org/10.1016/j.compstruct.2020.111898.
20. **Mao, Q.; Pietrzko, S.** 2013. Control of noise and structural vibration, Springer-Verlag London Ltd
21. **Rimašauskienė, R.; Jūrėnas, V.; Radzienski, M.; Rimašauskas, M.; Ostachowicz, W.** 2019. Experimental analysis of active–passive vibration control on thin-walled composite beam, Composite Structures, p. 223. https://doi.org/10.1016/j.compstruct.2019.110975.
22. **Bowen, C. R.; Giddings, P. F.; Salo, A. I. T.; Kim, H. A**. 2011. Modeling and characterization of piezoelectrically actuated bistable composites. IEEE Transactions on Ultrasonics, Ferroelectrics, and Frequency Control 58 (9): 1737–1750. https://doi.org/10.1109/TUFFC.2011.2011.
23. **Farah, S.; Anderson, D. G.; Langer, R.** 2016. Physical and mechanical mechanical properties of PLA, and their functions in widespread applications : A comprehensive review, Advanced Drug Delivery Reviews 107: 367–392. https://doi.org/10.1016/j.addr.2016.06.012.
24. **Valvez, S.; Santos, P.; Parente, J. M.; Silva, M. P.; Reis, P. N. B**. 2020. 3D printed continuous carbon fiber reinforced PLA composites: A short review. Procedia Structura-Integrity 25: 394–399. https://doi.org/10.1016/j.prostr.2020.04.056.
25. **Ferreira, R. T. L.; Amatte, I. C.; Dutra, T. A.; Bürger, D.** 2017. Experimental characterization and

micrography of 3D printed PLA and PLA reinforced with short carbon fibers,Composites Part B: Engineering 124: 88–100.
https://doi.org/10.1016/J.COMPOSITESB.2017.05.013
26. **Sharghi, H.; Bilgen, O.** 2022. Continuous electric field modeling of Macro-Fiber Composites for actuation and energy harvesting, International Journal of Mechanical Sciences, p. 213.
https://doi.org/10.1016/J.IJMECSCI.2021.106864.
27. **Lashin, M. M. A.; Saleh, W. S.; Alrowais, F**. 2020, Determination of Different structures' materials natural frequencies using fuzzy logic system, International Journal of Engineering and Advanced Technology 9(3): 723–727.
https://doi.org/10.35940/ijeat.b3641.029320.
28. **Miyashiro, D.; Taira, H.; Hamano, R.; Reserva, R. L.; Umemura, K.** 2020. Mechanical vibration of single-walled carbon nanotubes at different lengths and carbon nanobelts by modal analysis method, Composites Part C: 2.
https://doi.org/10.1016/J.JCOMC.2020.100028.
29. **Mahato, S.; Hazra, B.; Chakraborty, A.** 2020. Structural Monitoring and Maintenance, Structural Monitoring and Maintenance 7(4): 283.
https://doi.org/10.12989/SMM.2021.7.4.283
30. **Mahato, S.; Teja, M. V.; Chakraborty, A.** 2015. Adaptive HHT (AHHT) based modal parameter estimation from limited measurements of an RC-framed building under multi-component earthquake excitations, Structural Control Health Monitoring 22(7): 984–1001.
https://doi.org/10.1002/STC.1727.
31. **Mahato, S.; Chakraborty, A.** 2016. EKF based parameter identification of LTI system from seismic response measurements, Procedia Engineering 144: 360–365.
https://doi.org/10.1016/J.PROENG.2016.05.144.

A. Raza, S. Mahato, R. Rimašauskienė

ACTUATION PERFORMANCE OF MACRO FIBRE COMPOSITE (MFC) AS ACTUATOR IN VIBRATION REDUCTION OF CANTILEVER BEAMS

S u m m a r y

This study proposes a vibration suppression technique that uses piezoelectric material to restrict the dynamic amplitudes of a cantilever beam. The finite element analysis (FEA) model of the cantilever is created and incorporated with Macro Fiber Composite (MFC8507-P2) in the ANSYS framework. A comparative study has been performed using three different types of materials i.e., Polylactic acid (PLA), PLA with Short Carbon Fibers (PLA-SCF Composite), and PLA with Continuous Carbon Fibers (PLA-CCF Composite), for the beam. An external disturbance causes the beam to vibrate, and the MFC8507-P2 patch provides a counter-force to the structure to reduce vibrations. The MFC8507-P2 patch is placed at an appropriate location on each beam to suppress vibration induced by the initial fundamental modes. Modal analysis has been performed to find the natural frequencies and the contribution of each mode to the overall response under dynamic loading conditions. Transient structural analysis is performed to observe the influence of the MFC8507-P2 patch on vibration amplitude with time. Furthermore, frequency response analysis has been performed to determine the impact of the MFC8507-P2 patch on the vibration amplitude of the natural modes. The vibration response has been measured at the tip of the beam and the simulation results validate that the vibration amplitude decreases as the applied voltage increases.

Keywords: vibration amplitude, cantilever beam, Macro Fiber Composite (MFC), composite, modal analysis, voltage.

Received June 28, 2022
Accepted January 27, 2023